Full-Range Cartesian-Decoupled Impedance Control for Physical Human-Robot Interaction with Series-Elastic Space Robots

Samuel A. Sowell[1,2] and Gray C. Thomas[3]
Texas A&M University, College Station, Texas, 77843

Effective physical human-robot interaction in space exploration is built on a foundation of admittance and impedance-controlled manipulators. Series-elastic actuators enable these manipulators to render compliant behaviors that are ideal for safe and responsive interaction. However, the cascaded control architectures commonly used in space robotics enforce a strict bandwidth hierarchy, requiring low-level position or torque control loops to operate significantly faster than high-level admittance or impedance loops. This constraint limits achievable performance by preventing the manipulator from expressing the full range of its potential impedance behaviors. Leveraging recent advancements in spaceflight computing, we present a non-cascaded, state-space full-state feedback control architecture that removes the bandwidth hierarchy requirement. This approach enables simultaneous realization of stiff, compliant, and natural impedance behaviors across multiple Cartesian degrees of freedom, a capability we call Full-Range Cartesian-Decoupled Impedance Control. The approach is validated in simulation on a three-degree-of-freedom NASA Valkyrie upper-arm testbed with series-elastic joints. Comparative experiments with a conventional cascaded controller demonstrate a wider stable impedance range, expanding the spectrum of safe human-robot collaboration behaviors for future space missions.

Acronyms and Nomenclature

DLR	=	German Aerospace Center
DOF	=	Degree-of-Freedom
EVA	=	Extravehicular Activity
FR-CDIC	=	Full-Range Cartesian-Decoupled Impedance Control
FSF	=	Full-State Feedback
IVA	=	Intravehicular Activity
OSAM	=	On-Orbit Servicing, Assembly, and Manufacturing
SEA	=	Series-Elastic Actuator

[1] PhD Student, Department of Mechanical Engineering, JCAIN 111, 180 Spence St, College Station, TX 77840.
[2] Robotics Engineer, Robotic Systems Technology Branch, 2101 NASA Parkway, Mail Code ER4.
[3] Assistant Professor, Department of Mechanical Engineering, MEOB 110, 180 Spence St, College Station, TX 77840.

Trade names are used in this presentation for identification only. Their usage does not constitute an official endorsement, either expressed or implied, by the National Aeronautics and Space Administration.

I. Introduction

FUTURE human spaceflight missions will increasingly rely on robotic systems that physically interact with astronauts, tools, and spacecraft structures. Robots are expected to support intravehicular activities (IVA) [1] [2], extravehicular activities (EVA) [3], on-orbit servicing, assembly, and manufacturing (OSAM) [4], and surface operations [5], where direct physical contact between humans and robots is unavoidable. In these settings, safety, predictability, and intuitive physical behavior are as critical as precision and strength.

Historically, space manipulators such as the Canadarm family have been controlled using high-gain, position-based architectures designed for free-space operation and accurate trajectory execution [6]. While highly effective for large-scale manipulation and capture tasks, these systems exhibit inherently high output impedance. As a result, they are poorly suited for sustained physical interaction with humans or delicate structures, where contact forces must be regulated rather than rejected. As future missions place humans and robots in closer physical proximity, this limitation becomes increasingly restrictive.

Series-elastic actuators (SEAs) provide a promising hardware solution to this challenge by introducing intentional compliance between the motor and the joint [7]. By storing and releasing energy through an elastic element, SEAs enable impact mitigation, direct torque sensing, and stable force regulation. These properties make SEAs particularly attractive for space robotics, where uncertainty, limited situational awareness, and safety-critical interaction are dominant concerns. However, the inclusion of an elastic element fundamentally alters the actuator dynamics. For each degree of freedom, the coupled motor-spring-joint structure forms a fourth-order dynamical system, increasing both the dynamic complexity and the difficulty of control design.

To manage this complexity, SEA-equipped space robots are commonly controlled using cascaded impedance or admittance architectures [8] [9]. In cascaded impedance control, a fast inner torque loop is wrapped by a slower outer position loop that shapes joint (or Cartesian, end-effector) impedance. In admittance control, measured interaction forces are integrated into an outer loop to generate motion commands, which are sent to a fast inner position loop. Both approaches rely on a strict bandwidth hierarchy, in which the inner loop must operate significantly faster than the outer interaction dynamics. When this time-scale separation is maintained, the higher-order actuator dynamics can be abstracted away, simplifying analysis and implementation. However, this abstraction fundamentally limits achievable interaction performance. As desired stiffness reaches the extremes of the hardware capabilities, the outer loop begins to demand joint-level dynamics that approach or exceed the response capability of the inner loop. In this regime, elastic energy stored in the transmission becomes increasingly difficult to regulate, leading to oscillatory behavior or instability. As a result, cascaded impedance and admittance controllers often destabilize well before reaching the physical limits of the hardware, forcing SEA-based space robots to trade positional accuracy for compliance even when both can be achieved.

Alternatively, state-feedback control of SEA-based space robots has been explored to address cascaded architecture limitations. Work on the German Aerospace Center (DLR) lightweight robot series demonstrated globally stable full-state feedback (FSF) controllers that explicitly account for both motor and joint dynamics [10]. However, these approaches do not account for spring deflection rate and do not generalize.

Recent results in the single-degree-of-freedom case have shown that FSF control of SEAs can instead be designed and analyzed through pole placement and frequency-domain techniques [11]. In this formulation, the fourth-order actuator dynamics provide sufficient freedom to shape the closed-loop poles and zeros governing interaction behavior, enabling direct characterization of the impedance range permitted by physical constraints. These results reveal that many of the practical limits observed in cascaded impedance and admittance control arise from controller structure rather than from intrinsic hardware limitations.

Extending this insight to multi-degree-of-freedom manipulators is nontrivial due to coupled joint dynamics, configuration-dependent kinematics, and the need to preserve intuitive Cartesian behavior across the workspace. In this work, we present Full-Range Cartesian-Decoupled Impedance Control (FR-CDIC), a control framework that extends FSF SEA principles from the single-joint case to multi-degree-of-freedom space robots. Rather than employing state feedback solely as a stabilization mechanism, FR-CDIC uses it as a systematic design instrument. Feedback gains are synthesized under explicit impedance rendering constraints, enabling controlled shaping of the coupled actuator-joint dynamics. This formulation eliminates the bandwidth hierarchy inherent to cascaded impedance and admittance architectures and enables a single controller to span compliant, natural, and stiff interaction behaviors within hardware limits.

The proposed approach is validated experimentally within a high-fidelity dynamic simulation of a three-degree-of-freedom NASA Valkyrie upper-arm testbed with series-elastic joints [12]. Comparative experiments against a conventional cascaded impedance controller demonstrate a wider stable impedance range and more consistent

Cartesian behavior. These results indicate that FR-CDIC expands the practical interaction envelope of series-elastic space robots, providing a systematic and physically grounded path toward safe, intuitive, and high-performance human–robot interaction in future space missions.

II. Series-Elastic Actuator Dynamics

SEAs introduce a compliant element between the motor and the joint, fundamentally altering the internal dynamics of the actuation system. Mechanically, an SEA can be represented as a motor inertia coupled to a joint inertia through an elastic element. Motor torque produces deformation in the elastic element, and the resulting spring torque drives joint motion. During contact with the environment, energy is exchanged among the motor inertia, the elastic element, the joint inertia, and the external load. The elastic element temporarily stores mechanical energy and releases it as the interaction evolves. This storage-and-release mechanism underlies the impact mitigation and force controllability properties that motivate the use of SEAs in interaction-rich robotic systems.

However, a key dynamical consequence of this architecture is the increase in system order. For each degree of freedom, the motor inertia contributes second-order dynamics, and the joint inertia contributes second-order dynamics, yielding an effective fourth-order actuator-joint system. In contrast, rigidly actuated joints are typically modeled as second-order systems, with motor and joint coordinates treated as coincident. The additional states introduced by elasticity therefore represent additional dynamic degrees of freedom that directly influence closed-loop interaction behavior.

For a single degree of freedom, the SEA dynamics can be written as a linear system of scalars. Let θ_m denote motor position, θ_s the elastic deflection, and q the joint position, related by

$$q = \theta_m + \theta_s. \tag{1}$$

Assuming an ideal spring without damping or friction, the transmitted spring torque is

$$\tau_s = K_s \theta_s, \tag{2}$$

where K_s is the series-elastic spring stiffness. After applying partial feedback linearization to eliminate Coriolis and gravity terms,the simplified joint-side dynamics are

$$M\ddot{q} = -\tau_s + \tau_{ext}, \tag{3}$$

and the motor-side dynamics are

$$J_m\ddot{\theta}_m + B_m\dot{\theta}_m = \tau_s + \tau_m, \tag{4}$$

where J_m and M are motor and joint inertias, B_m is motor damping, τ_m is commanded motor torque, and τ_{ext} is external interaction torque. Together, these equations describe the fourth-order actuator-joint structure that governs force transmission and energy exchange.

FSF can be applied directly to this fourth-order system using a unified control law of the form

$$\tau_m = -K_1\theta_m - B_1\dot{\theta}_m + K_2\theta_s + B_2\dot{\theta}_s. \tag{5}$$

This controller uses proportional and derivative feedback from both the motor coordinate and the elastic deflection. The four gains K_1, B_1, K_2, and B_2 provide sufficient freedom to shape the effective second-order interaction behavior observed at the joint. In this interpretation, the additional states introduced by series elasticity are not a complication but an opportunity to expand the design space available for shaping interaction behavior. By selecting feedback gains subject to stability constraints, the fourth-order joint dynamics can be regulated to approximate a desired second-order behavior while preserving internal stability.

Extending this insight from a single joint to the general case of a multi-degree-of-freedom (DOF) manipulator requires a unified formulation that preserves the coupled actuator-joint dynamics across all joints. The following section develops the corresponding multi-DOF state-space model used for systematic control synthesis.

III. Multi-DOF System Modeling

To support systematic shaping of interaction dynamics, the coupled motor-spring-joint behavior of the series-elastic actuator is modeled explicitly using a unified, multi-degree-of-freedom state-space representation. This formulation preserves the full fourth-order dynamics introduced by series elasticity and provides direct access to all physically relevant states for control design. The series-elastic actuator dynamics are modeled using a linearized, multi-degree-of-freedom state-space representation that captures the coupled motor-spring-joint behavior. For each degree of freedom, the actuator contributes a fourth-order dynamic system consisting of second-order motor dynamics and second-order joint dynamics. The full system therefore contains $4n$ states for an n-degree-of-freedom manipulator.

For the multi-degree-of-freedom case, let $\theta_m \in \mathbb{R}^n$ denote the motor position vector, $\theta_s \in \mathbb{R}^n$ the elastic deflection vector, and $q \in \mathbb{R}^n$ the joint position vector, related by $q = \theta_m + \theta_s$. The transmitted spring torque is $\tau_s = K_s\theta_s$, where $K_s \in \mathbb{R}^{n\times n}$ is a diagonal matrix of series-elastic stiffnesses. The joint-side dynamics are $M\ddot{q} = -\tau_s + \tau_{ext}$, where $M \in \mathbb{R}^{n\times n}$ is the fully coupled joint-space inertia matrix and $\tau_{ext} \in \mathbb{R}^n$ represents external interaction torques. The motor-side dynamics are $J_m\ddot{\theta}_m + B_m\dot{\theta}_m = \tau_s + \tau_m$, where $J_m \in \mathbb{R}^{n\times n}$ is the diagonal reflected motor inertia matrix, $B_m \in \mathbb{R}^{n\times n}$ is the diagonal motor viscous damping matrix, and $\tau_m \in \mathbb{R}^n$ is the commanded motor torque. Together, these equations describe the coupled fourth-order actuator-joint dynamics for an n-degree-of-freedom series-elastic manipulator in motor–spring coordinates, largely mirroring the formulation for the single degree of freedom case.

Defining the state vector in motor-spring coordinates as

$$x = \begin{bmatrix} \theta_m \\ \dot{\theta}_m \\ \theta_s \\ \dot{\theta}_s \end{bmatrix} \in \mathbb{R}^{4n}, \tag{6}$$

the joint coordinate satisfies $q = \theta_m + \theta_s$. The measurable output vector is chosen as

$$y = \begin{bmatrix} q \\ \dot{q} \end{bmatrix} = \begin{bmatrix} \theta_m + \theta_s \\ \dot{\theta}_m + \dot{\theta}_s \end{bmatrix}. \tag{7}$$

Using the motor-side and joint-side dynamics together with $\tau_s = K_s\theta_s$, the open-loop system can be written in linear time-invariant state-space form as

$$\dot{x} = Ax + B_\tau\,\tau_m + B_\delta\,\tau_{ext}, \tag{8}$$

$$y = Cx, \tag{9}$$

where

$$A = \begin{bmatrix} 0 & I & 0 & 0 \\ 0 & -J_m^{-1}B_m & J_m^{-1}K_s & 0 \\ 0 & 0 & 0 & I \\ 0 & J_m^{-1}B_m & -(J_m^{-1}K_s + M^{-1}K_s) & 0 \end{bmatrix},\ B_\tau = \begin{bmatrix} 0 \\ J_m^{-1} \\ 0 \\ -J_m^{-1} \end{bmatrix},\ B_\delta = \begin{bmatrix} 0 \\ 0 \\ 0 \\ M^{-1} \end{bmatrix}, \tag{10}$$

and

$$C = \begin{bmatrix} I & 0 & I & 0 \\ 0 & I & 0 & I \end{bmatrix}. \tag{11}$$

Although SEAs require an extra encoder for spring deflection sensing, all states are directly measurable, enabling FSF without the use of observers. This formulation preserves the full fourth-order actuator-joint dynamics for each degree of freedom and serves as the foundation for gain synthesis and interaction shaping in the proposed control architecture.

IV. FR-CDIC Architecture

FR-CDIC is implemented as a non-cascaded FSF controller acting directly on the unified fourth-order motor-spring state representation. The motor torque command is generated from the full state vector (x, as defined in the last section) using a structured feedback law of the form

$$\tau_m = -Kx = -[K_1, V_1, K_2, V_2]x = -K_1\theta_m - V_1\dot{\theta}_m - K_2\theta_s - V_2\dot{\theta}_s, \tag{12}$$

where $K_1, K_2, V_1, V_2 \in \mathbb{R}^{n\times n}$ are gain matrices that may include off-diagonal coupling terms to shape multi-axis interaction behavior. (Note that this controller therefore relates the internal states of one joint to the motor current of another, leveraging high bandwidth communication between actuator controllers.) The formulation explicitly separates motor-side and elastic-side feedback contributions.

Substituting this control law into the motor-side dynamics

$$J_m\ddot{\theta}_m + B_m\dot{\theta}_m = K_s\theta_s + \tau_m, \tag{13}$$

yields an altered closed-loop dynamic equation for the motor

$$J_m\ddot{\theta}_m = (K_s - K_2)\theta_s - V_2\dot{\theta}_s - K_1\theta_m - (B_m + V_1)\dot{\theta}_m. \tag{14}$$

However, the spring and joint dynamics remain as before:

$$\tau_s = K_s\theta_s, \tag{15}$$

$$M(\ddot{\theta}_m + \ddot{\theta}_s) = -K_s\theta_s + \tau_{ext}. \tag{16}$$

In compact form, the closed-loop system becomes

$$\dot{x} = A_{cl}x + B_\delta\tau_{ext}, \tag{17}$$

with the new dynamic matrices expressible in block form as

$$A_{cl} = \begin{bmatrix} 0 & I & 0 & 0 \\ -J_m^{-1}K_1 & -J_m^{-1}(B_m + V_1) & J_m^{-1}(K_s - K_2) & -J_m^{-1}V_2 \\ 0 & 0 & 0 & I \\ J_m^{-1}K_1 & J_m^{-1}(B_m + V_1) & -(J_m^{-1}(K_s - K_2) + M^{-1}K_s) & J_m^{-1}V_2 \end{bmatrix}, \text{ and } B_\delta = \begin{bmatrix} 0 \\ 0 \\ 0 \\ M^{-1} \end{bmatrix}. \tag{18}$$

This closed-loop formulation preserves the full fourth-order actuator-joint dynamics for each degree of freedom while embedding the interaction-shaping gains directly into the system matrix. Unlike cascaded architectures, no inner-outer loop separation is imposed. Instead, the complete coupled motor–spring–joint dynamics are regulated as a single system.

The four gain matrices K_1, K_2, V_1, V_2 provide sufficient freedom to shape the dominant second-order interaction behavior perceived at the joints while simultaneously regulating internal actuator dynamics. The following section formalizes the gain-synthesis procedure, showing how Cartesian impedance objectives can be translated into structured feedback gains while guaranteeing closed-loop stability.

V. Impedance Rendering and Stability

The central objective of FR-CDIC is to select full-state feedback gains that produce a desired Cartesian impedance behavior while preserving internal stability of the complete fourth-order actuator–joint dynamics. Because the gains enter directly into the closed-loop state matrix, interaction behavior can be shaped explicitly through algebraic constraints derived from the SEA dynamics.

Impedance behavior is specified in Cartesian space, where stiffness and damping correspond directly to forces and motions experienced during physical human–robot interaction. Let the Cartesian wrench be $F \in \mathbb{R}^m$, and let the

manipulator Jacobian be $J(q) \in \mathbb{R}^{m\times n}$, mapping joint velocities to Cartesian velocities via $\dot{x} = J(q)\dot{q}$. The system is linearized about a fixed joint configuration q_0, and the Jacobian is evaluated at that point as $J_0 = J(q_0)$, yielding a local linear mapping between joint motion and Cartesian motion.

At the operating configuration, joint torque and Cartesian wrench are related by the torque relation

$$\tau_s = J_0^T F. \tag{19}$$

And the desired Cartesian interaction behavior is defined as

$$F = K_x(x - x_d) + V_x\dot{x}, \tag{20}$$

where $K_x, V_x \in \mathbb{R}^{m\times m}$are the desired Cartesian stiffness and damping matrices. Using the linearized kinematics

$$x - x_d = J_0(q - q_d), \dot{x} = J_0\dot{q}, \tag{21}$$

which, when substituted into the torque relation, gives the desired joint torque,

$$\tau_s = J_0^T K_x J_0(q - q_d) + J_0^T V_x J_0\dot{q}. \tag{22}$$

Under the FR-CDIC feedback structure, the SEA dynamics render effective joint-space stiffness and damping matrices derived from the closed loop dynamics (18),

$$K_{q,\text{eff}} = K_s(K_s + K_1 + K_2)^{-1}K_1, \tag{23}$$

$$V_{q,\text{eff}} = K_s(B_m + V_1 + V_2)^{-1}(B_m + V_1). \tag{24}$$

Thus, to enforce exact Cartesian impedance rendering at the operating configuration, we require

$$K_{q,\text{eff}} = J_0^T K_x J_0, \tag{25}$$
$$V_{q,\text{eff}} = J_0^T V_x J_0. \tag{26}$$

Rearranging the rendered effective stiffness and damping matrix system of equations to be affine yields

$$K_1\left(K_s^{-1}K_{q,\text{eff}} - I\right) + K_2\left(K_s^{-1}K_{q,\text{eff}}\right) = -K_{q,\text{eff}}, \tag{27}$$

$$V_1(K_s^{-1}V_{q,\text{eff}} - I) + V_2(K_s^{-1}V_{q,\text{eff}}) = B_m(I - K_s^{-1}V_{q,\text{eff}}) \tag{28}$$

These relations are affine in the decision variables K_1, K_2, V_1, and V_2, since K_s, B_m, J_0, K_x, and V_x are known matrices at the selected configuration. The gain synthesis problem is therefore posed as the convex optimization problem

$$\begin{aligned} &\min_{K_1,K_2,V_1,V_2} \quad \| K_1 \|_F^2 + \| K_2 \|_F^2 + \| V_1 \|_F^2 + \| V_2 \|_F^2, \\ \text{subject to} \quad &K_1(K_s^{-1}K_{q,\text{eff}} - I) + K_2(K_s^{-1}K_{q,\text{eff}}) = -K_{q,\text{eff}}, \\ &V_1(K_s^{-1}V_{q,\text{eff}} - I) + V_2(K_s^{-1}V_{q,\text{eff}}) = B_m(I - K_s^{-1}V_{q,\text{eff}}). \end{aligned} \tag{29}$$

The objective minimizes gain magnitude to avoid unnecessarily aggressive internal regulation, while the equality constraints enforce exact realization of the desired Cartesian stiffness and damping at the operating configuration.

After solving this convex program, the resulting gains are substituted into the closed-loop state matrix A_{cl}, and closed loop stability can be analyzed and verified with well-known state space methods. Importantly, the optimization is computationally efficient and suitable for real-time implementation, achieving an average solve time of 0.338 ms over 61,000 iterations, enabling operation at 2 kHz.

VI. Motivating Hardware Description

The experimental platform targeted for evaluation of FR-CDIC is a three-degree-of-freedom upper-arm robotic testbed derived from the NASA Valkyrie humanoid robot. Each joint is actuated through a series-elastic transmission, enabling compliant interaction, impact mitigation, and direct measurement of joint torque through elastic deflection. The testbed is representative of space-relevant manipulators intended for close physical interaction with astronauts, tools, and spacecraft structures.

The control system is implemented using a distributed, flight-representative architecture consisting of a centralized flight computer and joint-level motor control electronics. This separation reflects common practice in space robotics, where high-level control algorithms execute on a general-purpose processor while time-critical actuation and sensing are handled by dedicated hardware.

The FR-CDIC algorithm will execute on a PolarFire System-on-Chip (SoC) Icicle platform operating as the flight computer. The SoC runs a custom Yocto Linux operating system with the RT-PREEMPT patch and will evaluate the FR-CDIC control law at a fixed loop rate of 2 kHz. At each control cycle, the flight computer receives synchronized joint and actuator state measurements, computes joint commands, and generates current commands for each actuator. All impedance behavior will be synthesized at this level; with no impedance, admittance, or torque control loops implemented downstream of the flight computer. However, the low-level controllers may employ disturbance-observer-based friction compensation to better reproduce the ideal linear actuator dynamics experienced in simulators. While not required for stability, friction compensation enhances impedance fidelity by reducing low-velocity nonlinear effects.



Figure 1. Valkyrie Three-Degree-of-Freedom Testbed with PolarFire SoC Icicle Kit Flight Computer

Communication between the flight computer and the joint-level motor controllers is performed over an EtherCAT network operating at the same 2 kHz update rate. EtherCAT provides deterministic, low-latency communication and precise time synchronization between all devices on the network, ensuring coherent state feedback across all degrees of freedom. Sensor measurements and motor commands are exchanged in a single cyclic data frame, minimizing delay and jitter in the control loop.

Joint-level motor controllers are implemented using PolarFire FPGA fabric, which performs the low-level field-oriented control required for reliable actuation. These controllers operate as high-bandwidth current regulators and synchronized sensor interfaces rather than as nested control loops. Motor phase currents are regulated at a substantially higher internal rate, while position, velocity, and elastic deflection measurements are time-stamped and streamed to the flight computer each EtherCAT cycle. Joint torque is inferred from elastic deflection using the known series-elastic stiffness, eliminating the need for dedicated torque sensors.

This architecture intentionally avoids the traditional cascaded impedance structure in which motor controllers enforce high-bandwidth position or torque loops. Instead, the FPGA-based motor controllers act as deterministic current controllers with precise sensing, while all dynamic shaping of interaction behavior occurs in the centralized FR-CDIC controller. This arrangement allows the coupled motor-spring-joint dynamics to be regulated as a single system, removing the bandwidth hierarchy that constrains conventional SEA control architectures.

Although the present experiments rely on a ground-based testbed, the hardware configuration is representative of architectures used in existing and planned space robotic systems. The use of radiation-tolerant FPGA fabric for motion control, deterministic fieldbus communication, and centralized flight-computer-based control supports scalability to higher-degree-of-freedom manipulators and compatibility with future spaceflight implementations.

VII. Simulation Environment

Although the control architecture is flight-representative, comparative validation of FR-CDIC and conventional cascaded Cartesian impedance control was conducted in high-fidelity simulation. The hardware platform was replicated in NVIDIA Isaac Sim using PhysX-based rigid-body dynamics. Link inertias, motor reflected inertias,

viscous damping, and series-elastic stiffness values were set equal to characterized hardware parameters. Series elasticity was modeled explicitly as compliant rotational joints with specified stiffness and damping corresponding to the physical SEA transmissions and torque saturation limits matched hardware specifications. The simulation update rate matched the planned hardware update rate of 2 kHz for FR-CDIC and 500 Hz for the cascaded controller.

Both controllers were executed in soft real-time through the ROS 2 control framework and interfaced with the simulation model identically. No artificial damping, stabilization, or inner-loop compensation was introduced beyond specified physical parameters. Sensor noise and communication delay were not modeled in order to isolate structural controller effects. As a result, any observed oscillatory behavior or instability arises directly from the interaction between controller structure and the fourth-order SEA dynamics rather than from unmodeled disturbances.

This combined hardware-representative architecture and physics-consistent simulation environment provides a controlled and repeatable framework for evaluating how controller structure influences the achievable impedance range of series-elastic manipulators, acting as the foundation for the transfer to hardware for future testing and evaluation of FR-CDIC.

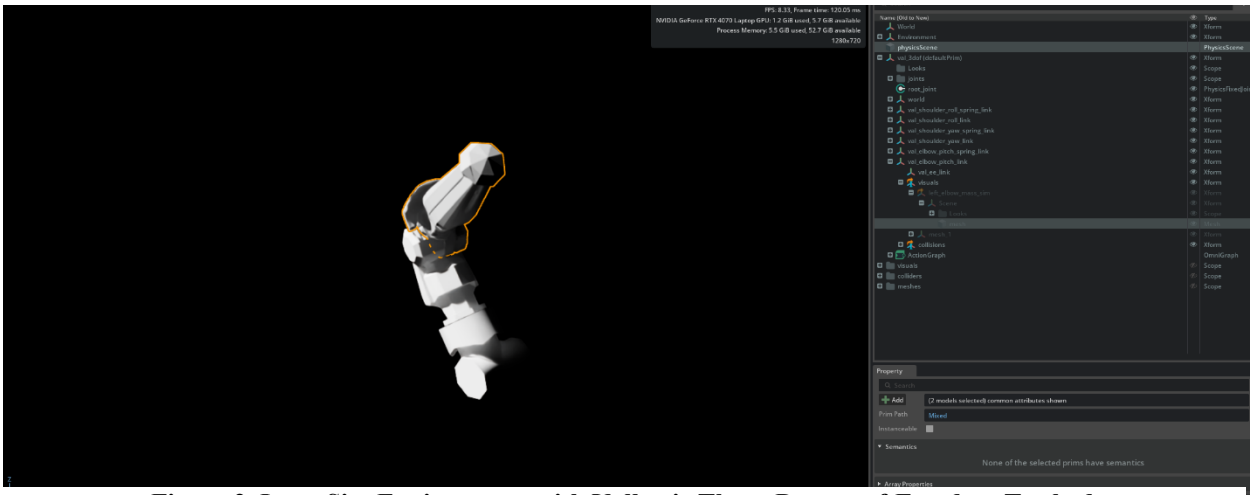


Figure 2. Isaac Sim Environment with Valkyrie Three-Degree-of-Freedom Testbed

VIII. Methods

To evaluate the proposed FR-CDIC framework, a comparative study was conducted against a conventional cascaded Cartesian impedance controller. Both controllers were implemented within the same high-fidelity simulation environment and operated under identical dynamic, kinematic, and actuator constraints to ensure structural comparability.

Both controllers render a desired second-order Cartesian impedance model in operational space. A Cartesian wrench of the form derived from Eq. (19) is computed and mapped to joint torques using the manipulator Jacobian and operational-space inertia formulation. This approach assumes that the inner torque dynamics that would be operating on the hardware are instantaneously realized in the simulation. However, the bandwidth hierarchy is consistently restricting the Cartesian impedance controller to run at 500 Hz. In contrast, FR-CDIC directly regulates the unified fourth-order motor–spring–joint state representation.

All experiments were conducted at a fixed manipulator configuration corresponding to a desired end-effector position of $x_0 = [0.03,\ 0.15,\ 0.55]^T$ meters. x_0 was chosen such that the Jacobian, J_0, is full rank and non-trivial. The desired Cartesian stiffness matrix contained a mix of stiff, neutral, and soft settings for each Cartesian direction:

$$K_x = \mathrm{diag}(300,\ 200,\ 100)\ \mathrm{N/m}, \tag{30}$$

and the damping ratio was set to $\zeta = 0.9$ for all Cartesian directions. For FR-CDIC, the corresponding Cartesian damping matrix was computed using the operational-space inertia evaluated at x_0.

Each trial began with the manipulator initialized at x_0. A Cartesian displacement via physical perturbation from the desired position was introduced to generate a transient interaction response. Each controller was then activated

and allowed to regulate the system for five seconds. End-effector position and Cartesian wrench were recorded throughout the trial. Plots were generated that overlayed the desired and actual Cartesian position and the desired and actual Cartesian wrench derived from the stiffness and damping matrices.

IX. Results

FR-CDIC demonstrated stable, well-damped behavior across all axes (Figure 3). External perturbations show position and torque tracking without compromising stability.

In contrast, the cascaded Cartesian impedance controller exhibited unstable behavior under the same impedance specification (Figure 4). While the controller was initially at rest prior to an external disturbance, oscillatory behavior emerged once the external perturbation was introduced.

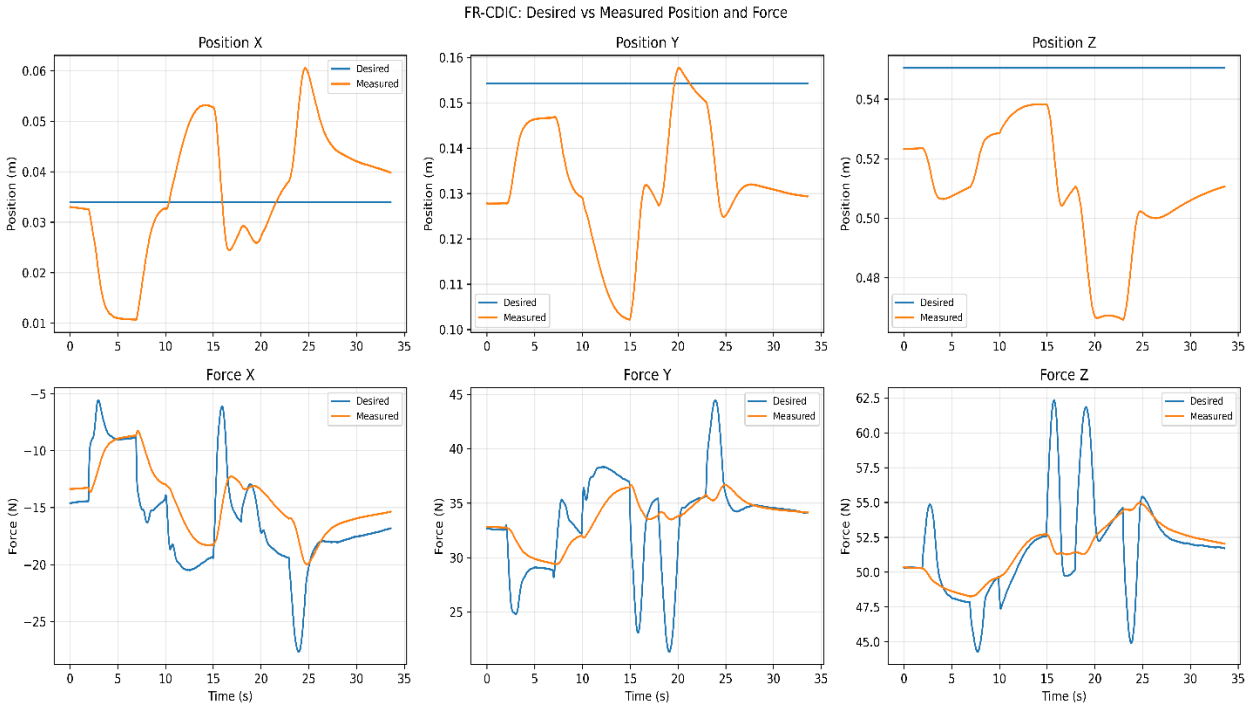


Figure 3. FR-CDIC controller response to external perturbations. Top row: Desired and measured end-effector position along the x, y, and z axes. Bottom row: desired and measured Cartesian forces, showing stable position and force tracking.

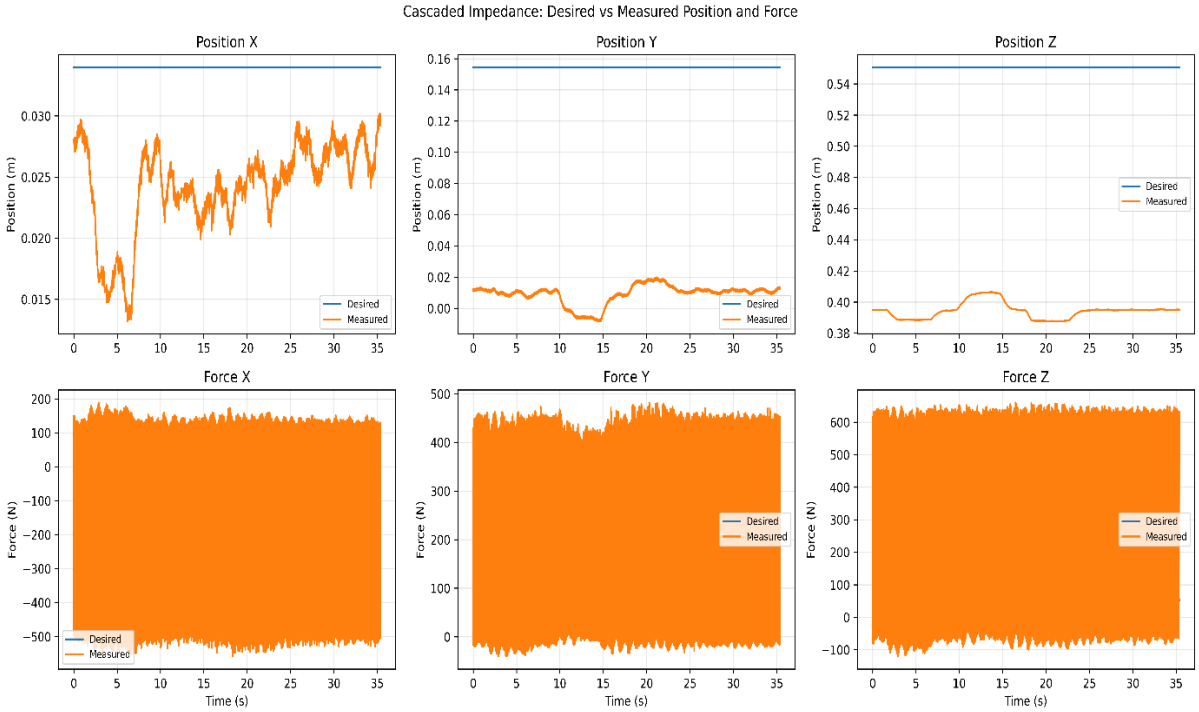


Figure 4. Cascaded Cartesian impedance controller response to external perturbations. Top row: Desired and measured end-effector position along the x, y, and z axes. Bottom row: desired and measured Cartesian forces, showing induced oscillatory instability at the commanded stiffness.

X. Discussion

The experimental results demonstrate that the proposed FR-CDIC framework can stably render Cartesian impedance behaviors that destabilize a conventional cascaded impedance controller under the same conditions. In the evaluated configuration, FR-CDIC produced well-damped position responses and force behavior consistent with the commanded impedance model, while the cascaded controller exhibited oscillatory force responses and degraded position tracking when subjected to the same perturbations. These observations highlight the potential of direct regulation of the coupled motor-spring-joint dynamics to widen the range of stable impedances that can be rendered by robots with series-elastic transmissions.

The primary implication of these results is that controller structure plays a significant role in determining the realizable impedance range of series-elastic manipulators. Cascaded impedance architectures rely on a strict bandwidth hierarchy in which the inner motor-level dynamics must operate significantly faster than outer interaction dynamics. When desired stiffness approaches the limits of the hardware, the bandwidth limitations imposed by the inner loop onto the outer loop result in unstable behavior. In contrast, FR-CDIC treats the motor and spring dynamics as a single system and regulates them simultaneously via FSF. This unified formulation allows the controller to realize stiffnesses not previously accessible.

However, several limitations should be noted when interpreting these findings. First, the comparative evaluation was performed in a controlled simulation environment designed to isolate structural controller effects. Sensor noise, communication delay, and friction effects were intentionally excluded from the simulation in order to focus on the controller design. While this approach verifies FR-CDIC viability for use on series-elastic space manipulators, additional experiments are required to quantify performance under realistic hardware conditions.

Second, experiments were conducted about a single operating configuration of the three-degree-of-freedom manipulator. Although the controller formulation is general, the results presented here do not establish stability or performance guarantees across the full workspace of the manipulator or for higher-degree-of-freedom systems. In the current implementation, the optimization is solved online at each control cycle within the 2 kHz loop, with gains recomputed at each cycle to account for configuration-dependent dynamics. While the convex structure is preserved

for higher-DOF manipulators, increasing to systems such as 7 DOF will introduce additional decision variables and constraints, leading to increased solve times; thus, real-time feasibility should be verified on the target hardware. Future work will examine the behavior of the controller across varying joint configurations and interaction scenarios.

Despite these limitations, the observed behavior displays encouraging evidence that FSF control of series-elastic manipulators can expand the interaction capabilities of space robotic systems. In applications involving physical human-robot interaction, such as IVA/EVA astronaut assistance, on-orbit servicing, and surface operations, robots must frequently transition between compliant and stiff behavior. A control architecture capable of spanning this range without switching control modes or enforcing strict bandwidth separation improves the predictability of robot interaction with their environments.

XI. Conclusion

This work presented Full-Range Cartesian-Decoupled Impedance Control (FR-CDIC), a non-cascaded full-state feedback control framework for series-elastic robotic manipulators. The approach directly regulates the coupled motor, spring, and joint dynamics to render desired Cartesian impedance behavior without relying on a strict bandwidth hierarchy required by conventional cascaded impedance controllers.

Comparative simulation experiments demonstrated that FR-CDIC can stably render Cartesian impedance behaviors that are simultaneously stiff, neutral, and soft in different axes, a goal that destabilized a cascaded Cartesian impedance controller under the same conditions. While the cascaded architecture exhibited oscillatory force responses and degraded position tracking under external perturbations, FR-CDIC maintained stable behavior consistent with the desired impedance model. These results support the elimination of bandwidth hierarchy constraints to allow series-elastic manipulators access to a wider range of stable impedance behaviors.

The proposed approach provides a systematic framework for shaping interaction dynamics in series-elastic space robots and may enable more capable physical human-robot interaction in future space missions. Ongoing work will extend the experimental evaluation to physical hardware and explore the behavior of the controller across a broader range of joint configurations and interaction scenarios.

References

[1] T. Ahlstrom, A. Curtis, M. Diftler, R. Berka, C. Joyce, J. Badger, and S. Yayathi, "Robonaut 2 on the International Space Station: Status update and preparations for IVA mobility," in *AIAA space 2013 conference and exposition*, 2013.

[2] S. Kang, R. Soussan, D. Lee, B. Coltin, Vargas, A.M., Moreira, M., K. Browne, R. Garcia, M. Bualat, T. Smith, and J. Barlow, "Astrobee iss free-flyer datasets for space intra-vehicular robot navigation research," *Robotics and Automation Letters,* vol. 9, no. 4, pp. 3307-3314, 2024.

[3] D. L. Akin and M. L. Bowden, "Eva, robotic, and cooperative assembly of large space structures," in *IEEE Aerospace Conference*, 2002.

[4] D. Arney, R. Sutherland, J. Mulvaney, D. Steinkoenig, C. Stockdale, and M. Farley, "On-orbit servicing, assembly, and manufacturing (OSAM) state of play," National Aeronautics and Space Administration (NASA), 2021.

[5] T. Fong, B. D. Allen and S. Azimi, *Autonomous systems & robotics for lunar surface infrastructure,* ASCEND, 2021.

[6] V. Abbasi, B. Azria, E. Tabarah, V. Menon, E. Phillips, and M. Bedirian, "Improved 7-DOF control of ISS robotic manipulators," in *Space OPS 2004 Conference*, 2004.

[7] G. A. Pratt and M. M. Williamson, "Series elastic actuators," in *IEEE/RSJ international conference on intelligent robots and systems. Human robot interaction and cooperative robots*, 1995.

[8] N. Paine, S. Oh, and L. Sentis, "Design and control considerations for high-performance series elastic actuators," *IEEE/ASME Transactions On Mechatronics,* vol. 19, no. 3, pp. 1080-1091, 2013.

[9] M. Diftler, J. Mehling, M. Abdallah, N. Radford, L. Bridgwater, A. Sanders, R. Askew, D. Linn, J. Yamokoski, F. Permenter, and B. Hargrave, "Robonaut 2-the first humanoid robot in space," in *IEEE international conference on robotics and automation*, 2011.

[10] A. Albu-Schäffer and G. Hirzinger, "A globally stable state feedback controller for flexible joint robots.," *Advanced Robotics,* vol. 15, no. 8, pp. 799-814, 2001.

[11] G. C. Thomas, J. S. Mehling, J. Holley, and L. Sentis, "Phase-relaxed-passive full state feedback gain limits for series elastic actuators," *IEEE/ASME Transactions on Mechatronics,* vol. 26, no. 1, pp. 586-591, 2020.

[12] N. Radford, P. Strawser, K. Hambuchen, J. Mehling, W. Verdeyen, A. Donnan, J. Holley, J. Sanchez, V. Nguyen, L. Bridgwater, and R. Berka, "Valkyrie: Nasa's first bipedal humanoid robot," *Journal of Field Robotics,* vol. 32, no. 3, pp. 397-419, 2015.

[13] A. Albu-Schäffer and G. Hirzinger, ""A globally stable state feedback controller for flexible joint robots.," *Advanced Robotics,* vol. 15, no. 8, pp. 799-814, 2001.